HHS Public Access

Author manuscript

Hum Mutat. Author manuscript; available in PMC 2020 September 16.

Published in final edited form as:

Hum Mutat. 2019 December ; 40(12): 2377–2392. doi:10.1002/humu.23894.

CAPN5 genetic inactivation phenotype supports therapeutic inhibition trials

Katherine J. Wert[1], **Susanne F. Koch**[2], **Gabriel Velez**[1,3], **Chun-Wei Hsu**[4,5], **MaryAnn Mahajan**[1], **Alexander G. Bassuk**[6], **Stephen H. Tsang**[4,5], **Vinit B. Mahajan**[1,7]

[1]Omics Laboratory, Byers Eye Institute, Department of Ophthalmology, Stanford University, Palo Alto, California

[2]Department of Physiological Genomics, Biomedical Center, Ludwig Maximillian University, Munich, Germany

[3]Department of Ophthalmology, Medical Scientist Training Program, University of Iowa, Iowa City, Iowa

[4]Department of Ophthalmology, Edward S. Harkness Eye Institute, New York Presbyterian Hospital, New York, New York

[5]Departments of Ophthalmology, Pathology, and Cell Biology, Jonas Children's Vision Care and Bernard and Shirlee Brown Glaucoma Laboratory, Institute of Human Nutrition, College of Physicians and Surgeons, Columbia Stem Cell Initiative (CSCI), Columbia University, New York, New York

[6]Department of Pediatrics, University of Iowa, Iowa City, Iowa

[7]Department of Ophthalmology, Veterans Affairs, Palo Alto Health Care System, Palo Alto, California

Abstract

Small molecule pharmacological inhibition of dominant human genetic disease is a feasible treatment that does not rely on the development of individual, patient-specific gene therapy vectors. However, the consequences of protein inhibition as a clinical therapeutic are not well-studied. In advance of human therapeutic trials for *CAPN5* vitreoretinopathy, genetic inactivation can be used to infer the effect of protein inhibition in vivo. We created a photoreceptor-specific knockout (KO) mouse for *Capn5* and compared the retinal phenotype to both wild-type and an existing *Capn5* KO mouse model. In humans, *CAPN5* loss-of-function (LOF) gene variants were ascertained in large exome databases from 60,706 unrelated subjects without severe disease phenotypes. Ocular examination of the retina of *Capn5* KO mice by histology and electroretinography showed no significant abnormalities. In humans, there were 22 LOF *CAPN5*

Correspondence: Katherine J. Wert and Vinit B. Mahajan, Department of Ophthalmology, Omics Laboratory, Byers Eye Institute, Stanford University, Palo Alto, CA, 94304. kjwert@stanford.edu (K. J. W.) and vinit. mahajan@stanford.edu (V. B. M.).

CONFLICT OF INTERESTS

The authors declare that there are no conflict of interests.

SUPPORTING INFORMATION

Additional supporting information may be found online in the Supporting Information section.

variants located throughout the gene and in all major protein domains. Structural modeling of coding variants showed these LOF variants were nearby known disease-causing variants within the proteolytic core and in regions of high homology between human CAPN5 and 150 homologs, yet the LOF of CAPN5 was tolerated as opposed to gain-of-function disease-causing variants. These results indicate that localized inhibition of CAPN5 is a viable strategy for hyperactivating disease alleles.

Keywords

ADNIV; calpain-5; gene therapy; human gene variants; loss-of-function; retina

1 | INTRODUCTION

Human gene therapy has gained success for cases of the autosomal recessive disease. These validated gene therapies, such as the first-ever *RPE65* gene therapy clinical trial, supplement diseased genes with wild-type (WT) copy (Pennesi et al., 2018; Russell et al., 2017). However, even the most successful gene supplementation therapy cannot address dominant mutations. To cure gain-of-function (GOF) disease mutations caused by autosomal dominant genes, the ultimate strategy is to correct the genomic DNA, which is now achievable through the CRISPR/Cas9 system. However, concerns have arisen about the low efficiency and safety of this strategy due to numerous off-target effects after delivery (Cho, Schaefer, Bassuk, Tsang, & Mahajan, 2018; Kosicki, Tomberg, & Bradley, 2018). Additionally, each patient must be sequenced, and their mutation must be known to be able to receive this therapy, and this requires a costly and unique treatment for each individual patient. To circumvent the cost and inefficiency of creating individual, patient-specific genetic therapies, a treatment option is needed that would impact autosomal dominant disease genes regardless of their specific mutations. One possible therapeutic approach for autosomal dominant disorders is the use of small molecule pharmacological inhibitors directed toward the mutated protein. On the basis of the success of ophthalmic gene therapy clinical trials, the ease of access to the eye, and the ability to inject intravitreally without the patient undergoing a major surgical procedure, clinical trials related to ophthalmic disease would be the ideal test for these small molecule inhibitors.

Previously, we have determined that GOF mutations in *CAPN5* cause a rare, dominantly inherited neovascular inflammatory vitreoretinopathy (NIV; MIM# 193235; Mahajan et al., 2012; Cham et al., 2016; Mahajan, Skeie, et al., 2012; Mahajan & Lin, 2013; Randazzo, Shanks, Clouston, & MacLaren, 2017). Most patients suffer nonsyndromic vision loss due to severe autoinflammatory uveitis, retinal neovascularization, and retinal degeneration. In the syndromic form, there is also hearing loss and developmental delay (Velez et al., 2018). *CAPN5* encodes the calcium-activated cysteine protease calpain-5, found to be ubiquitously expressed in the body, including in the eye (Schaefer et al., 2016). All NIV alleles change a single amino acid and reduce the calcium concentration required for activation, so the protease is hyperactive in disease (Bassuk et al., 2015; Gakhar et al., 2016). The majority of NIV alleles (RefSeq NM_004055.4; c.728G > T, p.Arg243Leu; c.731T > C, p.Leu244Pro; c.750G > T, p.Lys250Asn; c.799G > A, p.Gly267Ser; c.865C > T, p.Arg289Trp) fall within

the proteolytic core (subdomain PC2) of CAPN5. Only one mutation leading to a mild form of NIV (c.1126G > A, p.Gly376Ser) has been discovered in another noncatalytic domain of CAPN5 (domain III; CBSW; Randazzo et al., 2017).

We have previously modeled the proteolytic core of calpain-5 (both domains PC1 and PC2) and found that CAPN5 contains a calcium-sensitive, flexible gating loop that controls access to the catalytic groove (Bassuk et al., 2015). CAPN5 remains in its inactive state in the absence of calcium, where the two subdomains of the proteolytic core (PC1 and PC2) adopt an open conformation and prevent the formation of the catalytic triad (Gakhar et al., 2016). However, the structural modeling and small-angle X-ray scattering (SAXS) data highlight the complexity of CAPN5 regulation and our need for further understanding of its activation mechanism.

To examine the specific allelic mutations leading to autosomal dominant (AD) NIV in patients, we made mouse models for the p.Arg243Leu *CAPN5* mutation found in the first two ADNIV families (Wert et al., 2015; Wert, Skeie, Bassuk, Olivier, Tsang, & Mahajan, 2014). Mice carrying this *CAPN5* GOF allele were used to successfully recapitulate the human eye disease. Viral gene transfer of a mutant *CAPN5* allele and a transgenic mouse expressing mutant human *CAPN5* in the retina displayed features of autoinflammatory uveitis and retinal degeneration (Wert et al., 2015; Wert, Skeie, et al., 2014). In both model systems, expression of mutant *CAPN5* was driven by an opsin promoter, and therefore, limited to the rod photoreceptor cells. However, the rod expression alone of mutant human *CAPN5* was able to drive the ADNIV clinical phenotype. Thus, clinical treatments for ADNIV patients can benefit from the ability to localize them to the region of the eye, and in particular, the retina.

Current treatments for ADNIV patients have focused on controlling specific downstream clinical symptoms, but these therapies have not been able to inhibit all aspects of the disease phenotype or progression. For instance, local immunosuppression with steroids can treat early inflammatory symptoms of ADNIV, but the later fibrotic response and retinal degeneration persist in these patients (Mahajan, Tlucek, Folk, & Sobol, 2013; Velez, Bassuk, Colgan, Tsang, & Mahajan, 2017). Therefore, treatment of CAPN5-related disease will require inhibiting its activity, either by gene therapy or by small molecules (Nelson et al., 2014; Wang, Zhang, Song, & Gu, 2017). Inhibition of hyperactive CAPN5 should return CAPN5 activity to normal levels in a patient, but the concern is whether there would be adverse effects to the eye if CAPN5 activity is reduced below normal biological levels within the retina. In each case, there is a concern that the total suppression of CAPN5 activity might suppress other essential functions of CAPN5 in the eye or throughout the body.

Results from studies examining knockout (KO) mouse models of *Capn5* have been debated. One study of a previous *Capn5* KO mouse did not show any phenotype, with the exception of an increase in runts that passed away within 3–8 weeks after birth (Franz, Winckler, Boehm, & Dear, 2004). However, a comprehensive physiological examination was not performed, and the eye was not specifically examined. In a second study, embryonic lethality in homozygotes was observed by E3.5 after the mating of heterozygous mice

(Jackson Laboratory: 005784; Mouse Genome Informatics [MGI]: 3604529). In this model, the KO of *Capn5* displayed no eye abnormalities on a physical and histological exam. However, these KOs contained a reporter for β-galactosidase expression, and no lacZ was detectable in the eye of the mouse, so *Capn5* may not have been completely knocked out in this model.

To better understand the implications of *CAPN5* loss-of-function (LOF), specifically in the eye, we created a rod photoreceptor-specific KO model of *Capn5* and examined both heterozygous and homozygous KO mice from this line for any ocular abnormalities. We then validated the lack of adverse effects on visual function by examining the locations of human *CAPN5* LOF variants on the gene and protein structure. We found that the loss of *Capn5* within the photoreceptors of the eye does not cause detectable adverse clinical outcomes, and therefore inhibition of CAPN5 in the rod photoreceptor cells, even if it falls below normal, biological activity levels, is an efficacious strategy for future human clinical trials.

2 | MATERIALS AND METHODS

The study protocol was HIPAA (Health Insurance Portability and Accountability Act) compliant and adhered to the tenets of the Declaration of Helsinki. All animal experiments were performed in accordance with the ARVO Statement for the Use of Animals in Ophthalmic and Visual Research and were all approved by the Animal Care and Use Committee at Columbia University and Stanford University. All mouse experiments were run with a sample size of $N \geq 4$ mice, with both eyes examined per mouse.

2.1 | Gene and protein databases

All data from gene and protein databases presented in the manuscript were released publicly for the benefit of the wider biomedical community. Web resources used include the Exome Aggregation Consortium (ExAC) Browser (Beta; http://exac.broadinstitute.org), EsPript 3.0 (http://espript.ibcp.fr/ESPript/ESPript/), the NCBI Protein Database (https://www.ncbi.nlm.nih.gov/protein/), Online Mendelian Inheritance in Man (OMIM; https://www.omim.org), the Protein Database (PDB; https://www.rcsb.org/) and the University of California Santa Cruz (UCSC) Genome Browser (https://genome.ucsc.edu). Briefly, ENSG00000149260 was used for *CAPN5* in the Exome Aggregation Consortium (ExAC) database. The Human Feb. 2009 (GRCh37/hg19) Assembly for chromosome 11:76777979–76837201 in the UCSC genome browser was used for *CAPN5* and related analyses. RefSeq NM_004055.4 was used for *CAPN5.* Alignments were created by BLAST searches for CAPN5 in different species and then sequence alignments were performed using ClustalW (Thompson, Higgins, & Gibson, 1994). Sequence alignments were visualized using ESPript 3.0 (Robert & Gouet, 2018).

2.2 | Structural modeling of full-length human CAPN5

Homology models of CAPN5's protease core (PC1—PC2) were generated using MODELLER 9.14 (Eswar et al., 2006) with CAPN9 as a template as previously described and further refined by conformational sampling based on our previously published SAXS

data (Gakhar et al., 2016). Homology models of CAPN5's calpain β-sandwich domain (CBSW; DIII) were generated using CAPN2 as a template (PDB: 1KFU, 32% identity, 95% sequence coverage). Homology models of the CAPN5 C2 domain (DIV) were generated using the structure of the Munc13–1 C2 domain (PDB: 2CJT, 30% identity, 59% sequence coverage). Models of the individual domains were assembled using ab initio domain assembly in MODELLER to generate a model of the full-length CAPN5 structure. PyMOL generated all structural figures (The PyMOL Molecular Graphics System, Version 1.8; Schrödinger, LLC).

2.3 | ConSurf analysis

The structural model and sequence for human CAPN5 were used as input for analysis in the ConSurf server (Ashkenazy et al., 2016). Briefly, a position-iterated BLAST search (PSI-BLAST) against the UNIREF90 database (3 iterations) yielded 462 homologous sequences from vertebrates and invertebrates (378 unique sequences). The 150 closest homologous sequences to the query sequence with the lowest *E*-value (minimum sequence identity of 35%; *E*-value < 0.0001) were used for further analysis. These sequences underwent multiple sequence alignment using MAFFT (Katoh, Misawa, Kuma, & Miyata, 2002) and conservation scores were calculated using the Bayesian method option in ConSurf. The ConSurf scores were mapped onto the *B*-value column of the human CAPN5 structural model and visualized using PyMOL (The PyMOL Molecular Graphics System, Version 1.8; Schrödinger, LLC).

2.3.1 | Knockout mouse databases—Previous KO mouse phenotype data were retrieved from publicly available databases. Web resources used include the European Mutant Mouse Archive (EMMA; https://www.infrafrontier.eu/infrafrontier-research-infrastructure/international-collaborations-and-projects/european-mouse), the International Mouse Phenotyping Consortium (IMPC; http://www.mousephenotype.org/), The Jackson Laboratory (https://www.jax.org), the Knockout Mouse Project (KOMP; https://www.komp.org/), the Mary Lyon Centre (MRC) Harwell (https://www.har.mrc.ac.uk), and Mouse Genome Informatics (MGI; http://www.informatics.jax.org/).

2.4 | Generation of mutant mouse lines

Capn5$^{tm1a(EUCOMM)Hmgu}$ mice were obtained through the EMMA and the MRC Harwell (Oxfordshire, UK). Briefly, the targeted knockout *Capn5*$^{tm1a(EUCOMM)Hmgu}$ mice had an L1L2_Bact_P cassette inserted at position 98136457 of Chromosome 7 upstream of the critical exon 4 for *Capn5,* determined from Build GRCm38. The L1L2_Bact_P cassette is composed of an FRT site followed by lacZ sequence and a loxP site. This first loxP site is followed by neomycin under the control of the human beta-actin promoter, SV40 polyA, a second FRT site, and a second loxP site. A third loxP site is inserted downstream of *Capn5* exon 4 at position 98135489 so that exon 4 is flanked by loxP sites.

The *Pde6g-creERT2* mice were created as previously described (Koch et al., 2015, 2017). Briefly, *cre* is expressed in the photoreceptor cells of the retina and able to provide near-complete recombination 2 weeks after tamoxifen delivery (Koch et al., 2015, 2017). We have previously published a cross between the *Pde6g::creERT2* transgenic mouse to the

ROSA$^{nT–nG}$ reporter mouse line (Koch et al., 2017) where *ROSA*$^{nT–nG}$ mice contain a fluorescent allele that expresses nuclear-localized red fluorescence (tdTomato) in all cells, except those exposed to Cre recombinase; the latter cells express nuclear-localized enhanced green fluorescent protein. In *ROSA*$^{nT–nG}$ × *Pde6g::CreERT2* mice, red and green nuclei were uniformly distributed over the entire photoreceptor cell body-containing outer nuclear layer (ONL). Only red nuclei were found in the inner nuclear layer (INL), which does not contain photoreceptor cell bodies. The *Capn5*$^{tm1a(EUCOMM)Hmgu}$ mice were crossed with the *Pde6g-creERT2* mice to create homozygous and heterozygous *creERT2*-expressing *Capn5* knockout mice. Transgenic mice were identified by analyzing genomic DNA isolated from ear punches. Tissue was homogenized and digested extensively with proteinase K. The *Pde6g-creERT2* mice were genotyped as previously described (Koch et al., 2015, 2017). Polymerase chain reaction (PCR) primers for the *Capn5*$^{tm1a(EUCOMM)Hmgu}$ mice were designed based on the MRC Harwell Tm1a genotyping protocol to provide a WT band of 221 bp and a mutant band of 130 bp. Capn5–5arm-WTF: 5′ GGATGAGGAACCATGAGAGGG 3′; Capn5-Crit-WTR: 5′ CTCTTGTCTCCCTCCCCACCTAAG 3′; 5mut-R1: 5′ GAACTTCGGAATAGGAACTTCG 3′. PCR amplification was performed as follows: 1 cycle at 95°C for 1 min; 30 cycles at 95°C for 10 s, 60°C for 10 s, and 72°C for 1s; and 1 cycle at 72°C for 30 s.

2.5 | Tamoxifen injection

Tamoxifen (100 mg/ml in ethanol; Sigma-Aldrich T5648) was thoroughly mixed at 42°C, diluted with corn oil to a final concentration of 10 mg/ml, and then injected intraperitoneally at a concentration of 100 μg/g body weight on three consecutive days (1 injection/day), beginning at Day 12. Mice were analyzed at least 2 weeks post tamoxifen injection.

2.6 | Histochemical analyses

Histochemical analyses were performed as previously described (Wert Skeie, et al., 2014; Wert et al., 2015, 2016). Briefly, whole mouse eyes were enucleated at approximately 1 month of age and fixed in 2% paraformaldehyde for 30 min. Eyes then underwent a sucrose gradient (5%, 10%, 15%, 20%, and 30% sucrose in phosphate-buffered saline) followed by immersion in the optimal cutting temperature (OCT) buffer for cryopreservation. Eyes were frozen in OCT buffer at −80°C. Once frozen, OCT blocks containing the eyes were sectioned on a cryostat at the 10-micron thickness and placed onto slides for staining.

2.7 | Immunofluorescence

Immunofluorescence was performed as previously described (Wert Skeie, et al., 2014; Wert et al., 2015, 2016). Rabbit anti-CAPN5 (1:250, GTX108347; GeneTex) and Goat anti-rabbit Alexa Fluor 488 (1:1,000, ab150077; Abcam) were used for immunostaining. Sections were mounted with coverslips using mounting media containing 4′, 6-diamidino-2-phenylindole (DAPI; Fluoromount-G with DAPI; Thermo Fisher Scientific) to stain the nuclei of the retina. Sections were then imaged using a fluorescence microscope (Zeiss, Oberkochen, Germany) with 405 and 488-nm excitation and images were analyzed with Zen imaging software (Zeiss).

2.8 | Quantitative PCR (qPCR)

Mouse retinas were dissected as previously described (Wert, Davis, Sancho-Pelluz, Nishina, & Tsang, 2013; Wert Skeie, et al., 2014). Genomic DNA was extracted using a proteinase K digestion followed by isopropanol precipitation, a 75% ethanol wash, and resuspension in Tris-ethylenediaminetetraacetic acid buffer. Twenty-five nanograms of genomic DNA per sample were used for qPCR analysis to measure the presence of *Capn5.* To correct for sample-to-sample variations in qPCR efficiency and errors in sample quantification the amplification of *Gapdh* was used as an invariant endogenous control. Primers for *Capn5:* 5′ CCTTGGTGTTCTGAGCCCTTAGC 3′ and 5′ TGGTGAGCCTCACGTGTCACTC 3′ Primers for *Gapdh:* 5′ AGGTCGGTGTGAACGGATTTG 3′ and 5′ TGTAGACCATGTAGTTGAGGTCA 3′. All 4 samples were run in technical triplicates in a 384-well plate with Fast SYBR Green Master Mix (Life Technologies) using the QuantStudio 7 Flex Real-Time PCR System (Applied Biosystems). Experiments were replicated on a different day and new plate to ensure reproducibility of results. Relative quantification ratios were calculated and determined by $R = 2^{-\Delta\Delta Ct}$. For all experimental samples, relative quantification was measured in comparison with WT control mouse DNA samples from two different mouse genetic inbred backgrounds. Error bars represent the standard deviations of the technical triplicates.

2.9 | Immunoblot

Retinas were collected from adult mice, lysed in M-PER (Mammalian Protein Extraction Reagent; Thermo Fisher Scientific) containing cOmplete™ Protease Inhibitor Cocktail and sonicated. Protein concentrations were measured using the bicinchoninic acid (BCA) protein assay (Thermo Fisher Scientific). Proteins were separated by SDS-PAGE (4–15%; Bio-Rad), and transferred to nitrocellulose (Bio-Rad). After blocking, membranes were incubated in anti-Calpain-5 antibody (1:100, ab38943, Abcam) 3 hr at room temperature, washed, and then incubated in goat anti-rabbit immunoglobulin G–horseradish peroxidase (IgG–HRP) secondary antibody (1:2,000, sc-2004; Santa Cruz Biotechnology) for 1 hr at room temperature. Glyceraldehyde 3-phosphate dehydrogenase (GAPDH) loading control was detected using rabbit anti-GAPDH antibody (1:2,000, ab9485; Abcam) and goat anti-rabbit IgG–HRP secondary antibody (1:2,000, sc-2004; Santa Cruz Biotechnology). As for size standard, PageRuler Plus Prestained Protein Ladder (Thermo Fisher Scientific) was used. Membranes were visualized by chemiluminescence detection (Millipore), using BioMax film (Kodak).

2.10 | Electroretinography (ERG)

At 4–6 weeks of age, mice were dark-adapted overnight, manipulations were conducted under dim red light illumination, and recordings were made using Espion ERG Diagnosys equipment (Diagnosys LLL, Littleton, MA), as previously described (Wert et al., 2013, 2015; Wert, Sancho-Pelluz, et al., 2014; Wert, Skeie, et al., 2014). Mice were first anesthetized by IP injection of 0.1 ml/10 g body weight of anesthetic solution (1 ml of 100 mg/ml ketamine and 0.1 ml of 20 mg/ml xylazine in 8.9 ml of phosphate-buffered saline). Body temperature was maintained at 37°C using a heating pad. Mouse pupils were dilated by topical administration of 2.5% phenylephrine hydrochloride and 1% tropicamide.

Electrodes were placed on the corneas, and gonioscopic prism solution (Alcon) applied to each eye. ERG responses were recorded simultaneously from both eyes using an Espion Visual Electrophysiological System (Diagnosys). Rod and mixed rod–cone responses were recorded from dark-adapted mice using pulses of 0.001 and 3 cd·s/m^2 (white 6,500K), respectively. Then, mice were light-adapted for photopic responses for at least 10 min in the Ganzfeld dome. Recordings were carried out under rod-suppressing continuous background illumination of 30cd/m^2 (white 6,500K), Cone responses were recorded using pulses of 30 cd·s/m^2 (xenon).

2.11 | Statistical analyses

Differences in experimental groups were determined by one-way analysis of variance followed by Tukey's post-hoc multiple comparison's test. A $p < .05$ were considered significant.

3 | RESULTS

3.1 | Clinical phenotypes of *Capn5* knockout mice

Based on previous *Capn5* KO mice (MGI ID:4436604 and 3604529), it has been debated whether the loss of *Capn5* on both alleles could lead to an embryonic or early postnatal lethality. We mined the current data on *Capn5* in the IMPC, KOMP, EUCOMM (European Conditional Mouse Mutagenesis Program), and MGI databases (Blake et al., 2017; Dickinson et al., 2016). We found phenotyping for one specific *Capn5* KO mouse model: *Capn5*$^{tm1a(EUCOMM)Hmgu}$. In these mice, *Capn5* gene function was disrupted by a sequence insertion called the *tm1a* allele (Figure 1a); mice homozygous for the *tm1a* allele have a LOF of the *Capn5* gene.

Information on the *Capn5* KO mice is available on the IMPC database online (www.mousephenotype.org). Both male and female homozygotes for the *tm1a* disrupted *Capn5* allele showed a significantly increased acoustic startle reflex and prepulse inhibition (PPI; $p < .0001$; Figure 1b), which is a reduced threshold and/or more severe reflex response to stimuli, most often auditory stimulation (Blake et al., 2017). PPI reflects the ability of the mouse to integrate and inhibit sensory information, and the failure to do so has been shown in a variety of human neurological disorders, such as Huntington's disease and autism (Cadenhead, Carasso, Swerdlow, Geyer, & Braff, 1999; Ouagazzal, Grottick, Moreau, & Higgins, 2001; Ouagazzal, Jenck, & Moreau, 2001; Swerdlow, Braff, & Geyer, 1999). This correlates with human ADNIV patients, as recently we have shown that one GOF mutation, p.Arg289Trp causes a syndromic form of NIV with the presentation of hearing loss and developmental delay (Velez, et al., 2018). In the knockout mice, this startle reflex was slightly more significant in males (112 of 3,080; 3.64%) compared to females (97 of 3,070; 3.16%), although it did affect both genders (Blake et al., 2017). With the exception of the increased startle magnitude, other neurological symptoms were not found to be significantly altered in the *Capn5* KO mice (Figure 1c,d).

Additionally, both male and female homozygotes for the *tm1a* disrupted *Capn5* allele showed a significant increase in body weight ($p < .0001$; Figure 1e; Blake et al., 2017).

Previously, *CAPN5* gene variants in humans were shown to be associated with diastolic blood pressure and cholesterol levels, suggesting a role in cardiovascular disease and metabolic syndrome (Hohl-Abrahao & Creutzfeldt, 1991). *CAPN5* has also been linked to obesity through interaction with peroxisome proliferator-activated receptor delta (Saez et al., 2008). Although the auditory system (similar to symptomatic ADNIV human patients with the p.Arg289Trp mutation) and body weight (a possible role for *CAPN5* in metabolic syndrome and obesity) were significantly altered in these KO mice, examination of the eye showed no significant differences in the mice homozygous for the *tm1a* allele in *Capn5* (Figure 1f; Blake et al., 2017). However, only the anterior eye was examined for these mice, and thorough phenotyping of the retina was not included in the parameters tested. We have shown that *Capn5* is expressed in the retina, including the photoreceptor cells and synapses, and rod-specific expression of GOF CAPN5 mutations were enough to lead to ADNIV in a transgenic mouse model (Schaefer et al., 2016; Wert Skeie, et al., 2014; Wert et al., 2015). Therefore, it is important to examine the effect of CAPN5 LOF within the rod photoreceptor cells of the retina.

3.2 | Posterior eye health in tm1a *Capn5* knockout mice and photoreceptor-specific *Capn5* knockout mice

We obtained and examined $Capn5^{tm1a(EUCOMM)Hmgu}$ KO mice for retinal abnormalities and visual function. As it is possible that the *Capn5* gene could skip over the lacZ cassette in this *tm1a* allele, and lead to the restoration of gene function, we examined the *Capn5* KO mice for CAPN5 protein at 2.5 months of age. Using an antibody known to recognize CAPN5 protein within the inner retinal cell layers, we found that the *Capn5* KO mice had similar CAPN5 protein expression within the inner retina as a WT mouse (Figure 2a). Therefore, to specifically ablate CAPN5 in the photoreceptor cells, where GOF leads to the NIV disease phenotype, we crossed the *Capn5* KO mice to our previously published *Pde6g-creERT2* mouse line, with *cre* expressed in the rod photoreceptor cells of the retina and able to provide near-complete recombination 2 weeks after tamoxifen delivery (Figure 2b; Koch et al., 2015, 2017). The delivery of tamoxifen removes the critical exon 4 in the retinal cells and knocks out the gene function (Figure 2c).

To test for the loss of *Capn5* in the retinas from both the tm1a allelic mice and mice receiving tamoxifen to remove *Capn5* in the rod photoreceptor cells, we dissected retinas at postnatal Day 42 (P42) from both the *Capn5* KO mice and *Capn5* KO + tamoxifen mice and collected genomic DNA. We additionally extracted retinas from two separate WT control mice from both an agouti genetic background and C57BL/6J genetic background, as these are the two background variations that are found in the *Capn5* KO mice after cross-breeding. We then analyzed the retinal genomic DNA by qPCR for the relative expression of *Capn5* as normalized to *Gapdh* (Figure 2d). We found that compared to one of the WT retinas (from the C57BL/6J genetic background), the *Capn5* KO mice had a significant decrease in *Capn5* ($p = .0049$). However, some *Capn5* expression was still detectable within the retina. In contrast, the *Capn5* KO + tamoxifen mice displayed a significant decrease in *Capn5* expression in comparison to both WT samples ($p = .0104$ and $p = .0014$, respectively), at levels barely detectable by qPCR analysis.

We next examined the retinas for CAPN5 protein using western blot analysis in 2-month-old mice. Two weeks after tamoxifen injection, *Capn5* KO mice had 50.63% of CAPN5 protein compared to a WT control (Figure 2e). This suggested that CAPN5 is lost from the rod photoreceptor cells after tamoxifen injection, but still present within the inner retinal cell layers. Additionally, the eyes were cross-sectioned and stained with DAPI (Figure 2f–g). There was no detectable shortening of retinal cell layers, specifically the outer nuclear layer (ONL) containing the photoreceptors, between *Capn5* KO mice (Figure 2f, white arrows) and *Capn5* KO +tamoxifen mice (Figure 2g, white arrows).

Although the histological phenotype appeared normal, it was possible that mice at this time have a reduction in their visual response. For instance, during early stages of retinal disease, before human ADNIV patients suffer widespread photoreceptor degeneration, they show a loss of the scotopic and photopic electroretinogram (ERG) response, indicating inner retina signaling defects. To test whether this phenotype was present in our *Capn5* KO mice, ERG testing was performed at 6 weeks of age. Additionally, all mice undergoing live imaging via ERG underwent fundus examinations, and no abnormalities were visible using fundoscopy (data not shown). C57BL6/J WT mice (blue), heterozygous *Capn5* mice (green), *Capn5* KO mice (black), and *Capn5* KO + tamoxifen mice (purple) showed no differences in the recordings from the dark-adapted 3.0 maximal scotopic ERGs, dim-light scotopic ERGs for rod photoreceptor function, or photopic ERGs for cone photoreceptor function (Figure 3a). Quantification of the cohort of mice for each setting showed similar visual readouts between all four groups (Figure 3b–e). However, there was a significant increase in the a-wave maximal scotopic response for the *Capn5* KO + tamoxifen mice (purple) compared to both the WT mice (blue; $p = .0062$) and *Capn5* KO mice (black; $p = .0115$), but not the heterozygous *Capn5* mice (green; Figure 3b). There were no significant differences between all four groups in the b-wave maximal scotopic response ($p = .8056$; Figure 3c).

As the a-wave maximal scotopic response reflects the photoreceptor signaling, the rod- and cone-specific ERG recordings were analyzed. Although the a-wave maximal scotopic response detected a significant increase in the *Capn5* KO + tamoxifen mice (purple), there were no significant differences found in the cone-specific photopic response for these mice ($p = .1179$; Figure 3e). There were also no significant differences found in the mice for the rod-specific dim-light response ($p = .4045$; Figure 3d). The *Capn5* KO mice, both before and after tamoxifen injection, displayed only a mild increase in the maximal a-wave ERG recording, indicating a possible increase in visual response from the photoreceptor cells, and no detectable abnormalities or losses in retinal signaling responses. As the reduction in ERG is the earliest detectable phenotype in human patients, this suggests that targeted delivery of a CAPN5 inhibitor to the photoreceptors will not likely lead to adverse effects on visual function. However, it should be noted that ADNIV is a complex human disease that mimics various common blinding disorders, such as uveitis, retinitis pigmentosa, and diabetic vitreoretinopathy, and the effects of the LOF of CAPN5 in humans may not be fully translatable from a KO mouse model system.

3.3 | Nonpathogenic *CAPN5* gene variants in humans

Therefore, we interrogated human databases for LOF variants in *CAPN5.* Previously, we mapped gene variants for *CAPN5* from healthy individuals from 1000 Genomes and the Exome Variant Server (EVS; Schaefer et al., 2008). We found that most nonpathogenic *CAPN5* gene variants were located outside of the protease core of CAPN5. As GOF mutations in *CAPN5* lead to the NIV disease phenotype, we hypothesized that gene variants within the protease core were more likely to be pathogenic in comparison to variants that fall in the other domains. Recently, data from the Exome Aggregation Consortium (ExAC) has become publicly available (Lek et al., 2016). 1000 Genomes and EVS take into account data from 9,007 individuals, a smaller data set that exists in the ExAC browser, which provides gene variants from 60,706 unrelated individuals sequenced in various population genetic and disease-specific studies, that do not present with severe clinical disease phenotypes. We interrogated the ExAC browser for human *CAPN5* (ENSG00000149260; GRCh37/hg19; chr11:76777979–76837201). We found 880 variants, 22 of which were considered LOF variants for *CAPN5* (Table 1). The LOF variants lead to alterations in splice acceptor and donor sites, frameshift mutations, or early insertion of stop codons within the protein, all of which cause early termination of the protein during translation. All but three of the 22 LOF mutations were found on the canonical transcript (ENST00000278559), with three occurring on noncanonical transcripts for *CAPN5,* including one person with homozygous LOF of CAPN5. Additionally, 14 of the 22 LOF variants were considered rare (allele frequency, <0.001 and not a singleton), but the pLi score for all 22 LOF variants was equal to zero, suggesting tolerance for these LOF variants within human *CAPN5* and a decreased likelihood that these variants would be casual for clinical disease. Furthermore, the ExAC browser calculated a constraint metric z-score of −0.62 and −0.18 for synonymous and missense mutations, respectively, suggestive that these are tolerated within *CAPN5.* None of the GOF ADNIV mutations were found within the ExAC data set.

3.4 | Gene structure modeling of LOF splice-site and coding variants

We mapped the positions along chromosome 11 for each of the splice-site and coding variants found on the canonical transcript from the ExAC data set (Figure 4a). LOF mutations were found throughout the coding exons of *CAPN5* (exons 2–13), with the exception of exons 3, 5, 9, and 11. Missense mutations were also noted throughout the coding exons of *CAPN5.* Many mutations fell within exon 6, the same site where severe GOF mutations for ADNIV are located, and this exon encodes a part of the protease core of CAPN5. This suggests that the protease core may not harbor pathogenic mutations in comparison to the other domains, as we previously hypothesized, and analysis of the location of these tolerated gene variants on the protein structure of CAPN5 is needed.

3.5 | Structural modeling of LOF coding variants

Human CAPN5 is a nonclassical calpain family member, containing a protease core (domains PC1 and PC2), calpain β-sandwich domain (CBSW; domain III) and C2 domain (domain IV; Figure 4b). Published GOF mutations found in ADNIV-affected patients are located within the protease core of the protein, in domain PC2 (for the exception of one mutation causing a mild ADNIV phenotype, located within the noncatalytic CBSW

domain). The *CAPN5* LOF variants were found to affect amino acids within the protease core, CBSW domain, and C2 domain of the protein (red; Figure 4b). Interestingly, using the ExAC database, we found that gene variants also fell within the proteolytic core, near the sites of known ADNIV-causing GOF mutations (blue; Figure 4b).

We performed computer-based structural modeling to gain additional insight into the regions of CAPN5 affected by these LOF mutations. A model of the full-length CAPN5 protein was generated using a domain assembly approach. The structure of the protease core domain was modeled off the crystal structure for CAPN9 (PDB: 1ZIV; Davis et al., 2007) as previously described (Bassuk et al., 2015; Gakhar et al., 2016; Velez et al., 2018). The structure of CAPN5's CBSW domain (DIII) was modeled in the MODELLER 9.14 (Eswar et al., 2006) program using the crystal structure of human CAPN2 (Strobl et al., 2000) as a template (PDB: 1KFU, 32% identity, 95% sequence coverage). A total of five models were generated, which superimposed well within each group with major variations in the C-terminal region and minor variations in the loop regions (data not shown). The models had a root-mean-square standard deviation (RMSD) of 0.13–0.21 Å for 74 α carbon (Cα) atoms. A BLAST search for CAPN5's C2 domain (DIV) against the PDB returned structures of the Munc13–1 C2 domain as a top hit, with a sequence identity of 30% and coverage of 59% (PDB: 2CJT). Other close matches included C2 domains from the E3 ubiquitin ligase NEDD4 (PDB: 3BY7, 28% identity, 99% coverage) and NEDD4-like protein (PDB: 2NSQ, 24% identity, 99% coverage). Homology models of the CAPN5 C2 domain were generated using the structure of the Munc13–1 C2 domain (PDB: 2CJT). The models had an RMSD of 0.41–0.66 Å for 74 Cα atoms. Models of the individual domains were then assembled using ab initio domain assembly in MODELLER to generate a model of the full-length CAPN5 structure (Figure 4c; Velez, Tsang, Tsai, et al., 2017). Using this model, we were able to better visualize the location of LOF coding variants on CAPN5's domains (Figure 4d).

3.6 | Human variants fall in regions of high conservation across vertebrate species

It was possible that the gene variants within the protease core of CAPN5 were located at specific regions that were not highly conserved across species, in opposition to the conserved sites for the known GOF mutations leading to the clinical presentation of ADNIV. To further examine the conservation of these variants in CAPN5, amino acid sequences for each of the CAPN5 domains were aligned to specific vertebrates: rhesus, mouse, rat, rabbit, cow, cat, dog, chicken and frog CAPN5 protein sequences (Figures 5a and S1). Each of the tolerated LOF variants was found in highly conserved regions of CAPN5 in each of the domains, including the protease core (purple font; Figures 5a and S1). The sites of these variants were also nearby the highly conserved amino acids that are altered in ADNIV disease-causing mutations within DIII (blue font; Figure 5a). Missense mutations were also found within highly conserved regions of the protease core and other domains, including nearby sites to those of ADNIV disease-causing mutations (data not shown).

We next performed conservation analysis using our structural model of CAPN5 as an input into the ConSurf server. Briefly, a PSI-BLAST search against the UNIREF90 database returned 378 unique homologous sequences from vertebrates and invertebrates (35% minimum sequence identity). The 150 closest homologs were further analyzed by ConSurf

to produce conservation scores that were then mapped onto our structural model of CAPN5 (Figures 5b and S2). Variants with the highest conservation (magenta) were located within the protease core domain of CAPN5 (Figure 5b), in comparison to the variants found in other domains that were not as highly conserved (cyan) between the 150 sequences analyzed (Figure S2). Conservation scores were plotted for each of the LOF variants within the protease core (PC2) from the 150 analyzed homologous sequences (negative indicates conserved, positive indicates variable amino acid positions; Figure 5c).

To specifically examine conservation among vertebrates, and exclude invertebrate species, we utilized the 100 vertebrate base-wise conservation by PhyloP (phyloP100way) data for all 22 LOF variants listed in Table 1. Positive phyloP scores represent sites that are predicted to be conserved (magenta), and negative phyloP scores represent fast-evolving, nonconserved sites (cyan; Cooper et al., 2005; Kent et al., 2002). With the exception of one variant, the remaining 21 LOF gene variants showed positive phyloP scores, suggesting conservation across 100 vertebrate species within all domains of CAPN5 (Figure 5d). Thus, the LOF variants are found within highly conserved regions of CAPN5, and our original hypothesis, that the protease core and highly conserved regions were more likely to harbor disease-causing variants, was not accurate. Genetic mutations that lead to the loss of CAPN5 activity appear to be well-tolerated in both mice and humans in comparison to gene variants that lead to a gain in CAPN5 activity, which causes adverse disease effects such as NIV.

4 | DISCUSSION

Success in gene therapy for the autosomal recessive disease, specifically the *RPE65* Leber Congenital Amaurosis clinical trials in the eye, has shown that gene therapy is an ideal treatment option for patients (Pennesi et al., 2018; Russell et al., 2017). However, the delivery of a healthy gene allele is not feasible to treat patients with the autosomal dominant disease. Genetic editing with CRISPR/Cas9 is a new approach being studied as a therapeutic for dominant genetic mutations, but there have recently been safety concerns with the potential off-target cutting of DNA after delivery (Cho et al., 2018; Kosicki et al., 2018). Additionally, it is not possible to generate cost-effective therapeutic vectors for each individual patient mutation. Ideally, localized delivery of a small molecule inhibitor for the mutant gene would provide therapeutic effects for patients with a variety of mutations within alleles of that gene.

As molecular therapy has become feasible within the eye, it is crucial to understand what may occur in LOF conditions for a targeted gene. In cases of autosomal dominant inheritance patterns, as occurs for ADNIV caused by *CAPN5* mutations, future genetic editing approaches may knock out one or both alleles of the gene, and inhibitors will reduce the protein's function within the eye, each of which could lead to unwanted adverse side effects to the treated patient. For instance, another Mendelian disease, limb-girdle muscular dystrophy type 2A (MIM# 253600), is caused by the LOF of *CAPN3,* another member of the calpain family (Jia et al., 2001).

The inhibition of CAPN5 to treat patients is promising, as CAPN5 closely resembles its *Caenorhabditis elegans* homolog, *Tra-3,* and the reduction of *Tra-3* in *C. elegans* has been

shown to rescue inflammatory neuronal degeneration (Syntichaki, Xu, Driscoll, & Tavernarakis, 2002). Additionally, SNJ-1945, a small molecule inhibitor of calpains, rescued neuronal cell death in a model of traumatic brain injury as well as rescuing experimental autoimmune encephalitis (Bains et al., 2013; Trager et al., 2014). Inhibitors have also shown rescue effects for a variety of other common blinding disorders, such as retinitis pigmentosa (Ozaki et al., 2012, 2013), optic neuritis (Das et al., 2013; Smith et al., 2011), light-induced retinal toxicity (Imai, Shimazawa, Nakanishi, Tsuruma, & Hara, 2010; Kanan, Moiseyev, Agarwal, Ma, & Al-Ubaidi, 2007), retinal hypoxia (Hoang, Smith, & Senger, 2011; Shimazawa et al., 2010), retinal angiogenesis (Ma, Tochigi, Shearer, & Azuma, 2009) and diabetic retinopathy (Shanab et al., 2012). However, the specific inhibition of CAPN5, particularly in the eye, has not been thoroughly studied. Efforts have been made to develop CAPN5-specific inhibitors, but there are currently no CAPN5-specific inhibitors available.

The genetic LOF of CAPN5 is of particular importance as it is classified as a “nonclassical” calpain and lacks many of the calcium regulations that are found in other members of the calpain family. For all calpains, the calcium residues within the catalytic domain provide for a layer of calcium dependence. Furthermore, calpains in higher vertebrates have evolved a second regulatory layer by acquiring a calmodulin-like C-terminal domain (Bains et al., 2013). CAPN5, however, is more similar to *Tra-3,* and lacks this additional regulatory domain. Furthermore, CAPN5 is unable to form heterodimers with the regulatory subunit CAPNS1, and thus may rely more heavily on the calcium-binding within the protease core domain to control catalytic activity and could be more sensitive to alterations in expression levels (Campbell & Davies, 2012; Sorimachi, Ishiura, & Suzuki, 1997).

Instead of a reduction in CAPN5 via pharmacological inhibition, we examined mice for a full genetic inactivation of *Capn5,* using a knockout (KO) mouse model of *Capn5* and examining these mice for any retinal-specific clinical symptoms. As we found that residual *Capn5* was present in the retinas of these mice, we crossed these mice to a photoreceptor-specific *creERT2* mouse line to get full rod photoreceptor-specific loss of *Capn5.* Although no therapeutic approach will achieve 100% inhibition, these genetic mouse models can give us an idea if there are comorbidities with a significant reduction of enzyme activity, particularly within the disease-causing rod photoreceptor cells. We used both these mouse lines, including heterozygous mice, to examine the retinal phenotype. We found that the clinical and histological phenotype of the *Capn5* knockout and conditional photoreceptor KO mice is normal in all mice examined in this study. It is possible that the loss of CAPN5 could cause a slow degeneration phenotype that was not detected during the duration of our study. Another possible reason for this normal phenotype is that other calpains may compensate for the loss of CAPN5. In the retina, for example, there are eight other calpains expressed, which share homology with calpain-5 in the catalytic core (Schaefer et al., 2016; Suzuki, Hata, Kawabata, & Sorimachi, 2004). Additionally, it is possible that CAPN5 secreted from the inner retinal cells may compensate for the loss of CAPN5 within the photoreceptor cells, and CAPN5 inhibitors may need to be specifically localized to the photoreceptor cells for clinical therapeutics in human patients.

We did discern that the *Capn5* KO mice had an increase in breeding difficulties in comparison to WT controls. We found that some breeding pairs were unable to give birth to

pups, or if they did, the pups that were born had an increase in runted littermates who did not survive to weaning age. However, other breeding pairs from this same genetic background were able to conceive at a similar rate and litter size to WT controls. The breeding difficulties were quite variable in this line, and the strong breeding pairs were used to maintain the colony and provide the mice for our analysis. We have not found any mention of fertility loss in human patients with mutations within *CAPN5,* however, there is a possible link to polycystic ovary syndrome in females (González et al., 2006).

To validate the *Capn5* KO mouse model, we examined human databases for gene variants within *CAPN5*. Previously, we mined the 1000 Genomes and Exome Variant Server databases to estimate pathogenicity of *CAPN5* variants and predicted that <2% of *CAPN5* gene variants are damaging alleles. Using this data-mining approach, we found that most variants mapped to regions outside of the proteolytic core and hypothesized that mutations within the proteolytic core are particularly damaging (Schaefer et al., 2008). Here, we find that LOF and missense mutations in CAPN5 can fall within the proteolytic core and be tolerated, suggesting that the early termination of CAPN5 may not lead to a disease phenotype, and only mutations that lead to GOF alterations in CAPN5 enzymatic activity allow for an ADNIV clinical phenotype. In this current study, the increased ethnicities and individuals represented in the ExAC browser provide a more descriptive picture to determine the feasibility of future gene therapy approaches for ADNIV patients. By increasing our data-mining approaches from 9,007 to 60,706 individuals, we have an expansive view of the various gene variants found within *CAPN5* in the general population, without leading to severe clinical phenotypes.

Overall, the results from this study indicate that there are no major adverse clinical outcomes involved with photoreceptor-specific genetic inactivation of *CAPN5*, and therefore targeted suppression of CAPN5 is unlikely to lead to adverse outcomes in the eye. There may be a causal link to hearing loss, obesity, and fertility issues with systemic inhibition of CAPN5. However, the localized suppression of CAPN5 directly to the photoreceptor cells of the retina is a viable strategy and supports therapeutic inhibition trials.

Supplementary Material

Refer to Web version on PubMed Central for supplementary material.

ACKNOWLEDGMENT

V. B. M. and A. G. B. are supported by National Institutes of Health (NIH) grants (R01EY026682, R01EY024665, R01EY025225, R01EY024698, R21AG050437, and P30EY026877), and Research to Prevent Blindness (RPB), New York, NY. G. V. is supported by NIH grants (F30EYE027986 and T32GM007337). The Barbara & Donald Jonas Laboratory of Regenerative Medicine and Bernard & Shirlee Brown Glaucoma Laboratory are supported by the NIH (5P30EY019007 and R01EY018213), National Cancer Institute Core (5P30CA013696), the Research to Prevent Blindness (RPB) Physician-Scientist Award, unrestricted funds from RPB, New York, NY. S. H. T. is a member of the RD-CURE Consortium and is supported by the Tistou and Charlotte Kerstan Foundation, the Schneeweiss Stem Cell Fund, New York State (C029572), the Joel Hoffman Fund, the Professor Gertrude Rothschild Stem Cell Foundation, and the Gebroe Family Foundation.

REFERENCES

Ashkenazy H, Abadi S, Martz E, Chay O, Mayrose I, Pupko T, & Ben-Tal N (2016). ConSurf 2016: An improved methodology to estimate and visualize evolutionary conservation in macromolecules. Nucleic Acids Research, 44(W1), W344–W350. 10.1093/nar/gkw408 [PubMed: 27166375]

Bains M, Cebak JE, Gilmer LK, Barnes CC, Thompson SN, Geddes JW, & Hall ED (2013). Pharmacological analysis of the cortical neuronal cytoskeletal protective efficacy of the calpain inhibitor SNJ-1945 in a mouse traumatic brain injury model. Journal of Neurochemistry, 125(1), 125–132. 10.1111/jnc.12118 [PubMed: 23216523]

Bassuk AG, Yeh S, Wu S, Martin DF, Tsang SH, Gakhar L, & Mahajan VB (2015). Structural modeling of a novel CAPN5 mutation that causes uveitis and neovascular retinal detachment. PLOS One, 10(4), e0122352 10.1371/journal.pone.0122352 [PubMed: 25856303]

Blake JA, Eppig JT, Kadin JA, Richardson JE, Smith CL, & Bult CJ (2017). Mouse Genome Database (MGD)-2017: Community knowledge resource for the laboratory mouse. Nucleic Acids Research, 45(D1), D723–D729. 10.1093/nar/gkw1040 [PubMed: 27899570]

Cadenhead KS, Carasso BS, Swerdlow NR, Geyer MA, & Braff DL (1999). Prepulse inhibition and habituation of the startle response are stable neurobiological measures in a normal male population. Biological Psychiatry, 45(3), 360–364. [PubMed: 10023514]

Campbell RL, & Davies PL (2012). Structure-function relationships in calpains. Biochemical Journal, 447(3), 335–351. 10.1042/bj20120921 [PubMed: 23035980]

Cham A, Bansal M, Banda H, Kwon Y, Tlucek P, Bassuk A, … Mahajan A. (2016). Secondary glaucoma in *CAPN5*-associated neovascular inflammatory vitreoretinopathy. Clinical Ophthalmology, 10, 1187–1197. 10.2147/opth.s103324. [PubMed: 27390515]

Cho GY, Schaefer KA, Bassuk AG, Tsang SH, & Mahajan VB (2018). CRISPR genome surgery in the retina in light of off-targeting. Retina, 38(8), 1443–1455. 10.1097/iae.0000000000002197 [PubMed: 29746416]

Cooper GM (2005). Distribution and intensity of constraint in mammalian genomic sequence. Genome Research, 15(7), 901–913. 10.1101/gr.3577405 [PubMed: 15965027]

Das A, Guyton MK, Smith A, Wallace G, McDowell ML, Matzelle DD, … Banik NL (2013). Calpain inhibitor attenuated optic nerve damage in acute optic neuritis in rats. Journal of Neurochemistry, 124(1), 133–146. 10.1111/jnc.12064 [PubMed: 23106593]

Davis TL, Walker JR, Finerty PJ Jr., Mackenzie F, Newman EM, & Dhe-Paganon S (2007). The crystal structures of human calpains 1 and 9 imply diverse mechanisms of action and auto-inhibition. Journal of Molecular Biology, 366(1), 216–229. 10.1016/jjmb.2006.11.037 [PubMed: 17157313]

Dickinson ME, Flenniken AM, Ji X, Teboul L, Wong MD, White JK, … Murray SA (2016). High-throughput discovery of novel developmental phenotypes. Nature, 537(7621), 508–514. 10.1038/nature19356 [PubMed: 27626380]

Eswar N, Webb B, Marti-Renom MA, Madhusudhan MS, Eramian D, Shen M, … Sali A (2006). Comparative protein structure modeling using Modeller. Current Protocols in Bioinformatics, 15, 5.6.1–5.6.30. 10.1002/0471250953.bi0506s15

Franz T, Winckler L, Boehm T, & Dear TN (2004). Capn5 is expressed in a subset of T cells and is dispensable for development. Molecular and Cellular Biology, 24(4), 1649–1654. [PubMed: 14749380]

Gakhar L, Bassuk AG, Velez G, Khan S, Yang J, Tsang SH, & Mahajan VB (2016). Small-angle X-ray scattering of calpain-5 reveals a highly open conformation among calpains. Journal of Structural Biology, 196(3), 309–318. 10.1016/j.jsb.2016.07.017 [PubMed: 27474374]

González A, Sáez ME, Aragón MJ, Galán JJ, Vettori P, Molina L, … Ramírez-Lorca R. (2006). Specific haplotypes of the CALPAIN-5 gene are associated with polycystic ovary syndrome. Human Reproduction, 21(4), 943–951. 10.1093/humrep/dei443. [PubMed: 16396936]

Hoang MV, Smith LEH, & Senger DR (2011). Calpain inhibitors reduce retinal hypoxia in ischemic retinopathy by improving neovascular architecture and functional perfusion. Biochimica et Biophysica Acta (BBA)—Molecular Basis of Disease, 1812(4), 549–557. https://doi.Org/10.1016/j.bbadis.2010.08.008 [PubMed: 20804843]

Hohl-Abrahao JC, & Creutzfeldt OD (1991). Topographical mapping of the thalamocortical projections in rodents and comparison with that in primates. Experimental Brain Research, 87(2), 283–294. [PubMed: 1722758]

Imai S, Shimazawa M, Nakanishi T, Tsuruma K, & Hara H (2010). Calpain inhibitor protects cells against light-induced retinal degeneration. Journal of Pharmacology and Experimental Therapeutics, 335(3), 645–652. 10.1124/jpet.110.171298 [PubMed: 20823194]

Jia Z, Petrounevitch V, Wong A, Moldoveanu T, Davies PL, Elce JS, & Beckmann JS (2001). Mutations in calpain 3 associated with limb girdle muscular dystrophy: Analysis by molecular modeling and by mutation in m-calpain. Biophysical Journal, 80(6), 2590–2596. 10.1016/s0006-3495(01)76229-7 [PubMed: 11371436]

Kanan Y, Moiseyev G, Agarwal N, Ma JX, & Al-Ubaidi MR (2007). Light induces programmed cell death by activating multiple independent proteases in a cone photoreceptor cell line. Investigative Ophthalmology and Visual Science, 48(1), 40–51. 10.1167/iovs.06-0592 [PubMed: 17197514]

Katoh K, Misawa K, Kuma K, & Miyata T (2002). MAFFT: A novel method for rapid multiple sequence alignment based on fast Fourier transform. Nucleic Acids Research, 30(14), 3059–3066. [PubMed: 12136088]

Kent WJ, Sugnet CW, Furey TS, Roskin KM, Pringle TH, Zahler AM, & Haussler D (2002). The human genome browser at UCSC. Genome Research, 12(6), 996–1006. 10.1101/gr.229102 [PubMed: 12045153]

Koch SF, Duong JK, Hsu CW, Tsai YT, Lin CS, Wahl-Schott CA, & Tsang SH (2017). Genetic rescue models refute nonautonomous rod cell death in retinitis pigmentosa. Proceedings of the National Academy of Sciences of the United States of America, 114(20), 5259–5264. 10.1073/pnas.1615394114 [PubMed: 28468800]

Koch SF, Tsai YT, Duong JK, Wu WH, Hsu CW, Wu WP, … Tsang SH (2015). Halting progressive neurodegeneration in advanced retinitis pigmentosa. Journal of Clinical Investigation, 125(9), 3704–3713. 10.1172/jci82462 [PubMed: 26301813]

Kosicki M, Tomberg K, & Bradley A (2018). Repair of double-strand breaks induced by CRISPR-Cas9 leads to large deletions and complex rearrangements. Nature Biotechnology, 36(8), 765–771. 10.1038/nbt.4192

Lek M, Karczewski KJ, Minikel EV, Samocha KE, Banks E, Fennell T, … MacArthur DG (2016). Analysis of protein-coding genetic variation in 60,706 humans. Nature, 536(7616), 285–291. 10.1038/nature19057 [PubMed: 27535533]

Ma H, Tochigi A, Shearer TR, & Azuma M (2009). Calpain inhibitor SNJ-1945 attenuates events prior to angiogenesis in cultured human retinal endothelial cells. Journal of Ocular Pharmacology and Therapeutics, 25(5), 409–414. 10.1089/jop.2009.0030 [PubMed: 19857102]

Mahajan V, & Lin J (2013). Lymphocyte infiltration in CAPN5 autosomal dominant neovascular inflammatory vitreoretinopathy. Clinical Ophthalmology, 7, 1339–1345. 10.2147/opth.s46450 [PubMed: 23861576]

Mahajan V, Rowell AG, & Bassuk VB (2012). Monozygotic twins with CAPN5 autosomal dominant neovascular inflammatory vitreoretinopathy. Clinical Ophthalmology, 6, 2037–2044. 10.2147/opth.s40086 [PubMed: 23271883]

Mahajan VB, Skeie JM, Bassuk AG, Fingert JH, Braun TA, Daggett HT, … Stone EM (2012). Calpain-5 mutations cause autoimmune uveitis, retinal neovascularization, and photoreceptor degeneration. PLOS Genetics, 8(10), 10.1371/journal.pgen.1003001

Mahajan V, Tlucek PS, Folk JC, & Sobol WM (2013). Surgical management of fibrotic encapsulation of the fluocinolone acetonide implant in CAPN5-associated proliferative vitreoretinopathy. Clinical Ophthalmology, 7, 1093–1098. 10.2147/opth.s43939 [PubMed: 23785231]

Nelson NG, Skeie JM, Muradov H, Rowell HA, Seo S, & Mahajan VB (2014). CAPN5 gene silencing by short hairpin RNA interference. BMC Research Notes, 7, 642 10.1186/1756-0500-7-642 [PubMed: 25216694]

Ouagazzal A, Grottick AJ, Moreau J, & Higgins GA (2001). Effect of LSD on prepulse inhibition and spontaneous behavior in the rat. A pharmacological analysis and comparison between two rat strains. Neuropsychopharmacology, 25(4), 565–575. 10.1016/s0893-133x(01)00282-2 [PubMed: 11557170]

Ouagazzal AM, Jenck F, & Moreau JL (2001). Drug-induced potentiation of prepulse inhibition of acoustic startle reflex in mice: A model for detecting antipsychotic activity? Psychopharmacology, 156(2–3), 273–283. [PubMed: 11549229]

Ozaki T, Ishiguro S, Hirano S, Baba A, Yamashita T, Tomita H, & Nakazawa M (2013). Inhibitory peptide of mitochondrial μ-calpain protects against photoreceptor degeneration in rhodopsin transgenic S334ter and P23H rats. PLOS One, 8(8), e71650 10.1371/journal.pone.0071650 [PubMed: 23951212]

Ozaki T, Nakazawa M, Yamashita T, Sorimachi H, Hata S, Tomita H, … Ishiguro S (2012). Intravitreal injection or topical eye-drop application of a μ-calpain C2L domain peptide protects against photoreceptor cell death in Royal College of Surgeons' rats, a model of retinitis pigmentosa. Biochimica et Biophysica Acta (BBA)—Molecular Basis of Disease, 1822(11), 1783–1795. 10.1016/j.bbadis.2012.07.018 [PubMed: 22885154]

Pennesi ME, Weleber RG, Yang P, Whitebirch C, Thean B, Flotte TR, … Chulay JD (2018). Results at 5 years after gene therapy for RPE65-deficient retinal dystrophy. Human Gene Therapy, 29, 1428–1437. 10.1089/hum.2018.014 [PubMed: 29869534]

Randazzo NM, Shanks ME, Clouston P, & MacLaren RE (2017). Two novel CAPN5 variants associated with mild and severe autosomal dominant neovascular inflammatory vitreoretinopathy phenotypes. Ocular Immunology and Inflammation, 27, 693–698. 10.1080/09273948.2017.1370651 [PubMed: 29040051]

Robert X, & Gouet P (2014). Deciphering key features in protein structures with the new ENDscript server. Nucleic Acids Research, 42(Web Server issue), W320–W324. 10.1093/nar/gku316 [PubMed: 24753421]

Russell S, Bennett J, Wellman JA, Chung DC, Yu ZF, Tillman A, … Maguire AM (2017). Efficacy and safety of voretigene neparvovec (AAV2-hRPE65v2) in patients with RPE65-mediated inherited retinal dystrophy: A randomised, controlled, open-label, phase 3 trial. The Lancet, 390(10097), 849–860. 10.1016/s0140-6736(17)31868-8

Saez ME, Grilo A, Moron FJ, Manzano L, Martinez-Larrad MT, Gonzalez-Perez A, … Serrano-Rios M (2008). Interaction between Calpain 5, Peroxisome proliferator-activated receptor-gamma and Peroxisome proliferator-activated receptor-delta genes: A polygenic approach to obesity. Cardiovascular Diabetology, 7, 23 10.1186/1475-2840-7-23 [PubMed: 18657264]

Schaefer KA, Toral MA, Velez G, Cox AJ, Baker SA, Borcherding NC, … Mahajan VB (2016). Calpain-5 expression in the retina localizes to photoreceptor synapses. Investigative Ophthalmology and Visual Science, 57(6), 2509–2521. 10.1167/iovs.15-18680 [PubMed: 27152965]

Shanab AY, Nakazawa T, Ryu M, Tanaka Y, Himori N, Taguchi K, … Yamamoto M. (2012). Metabolic stress response implicated in diabetic retinopathy: The role of calpain, and the therapeutic impact of calpain inhibitor. Neurobiology of Disease, 48(3), 556–567. 10.1016/j.nbd.2012.07.025 [PubMed: 22967911]

Shimazawa M, Suemori S, Inokuchi Y, Matsunaga N, Nakajima Y, Oka T, … Hara H (2010). A novel calpain inhibitor, ((1S)-1-((((1S)-1-Benzyl-3-cyclopropylamino-2,3-di-oxopropyl)amino)carbonyl)-3-me thylbutyl)carbamic acid 5-methoxy-3-oxapentyl ester (SNJ-1945), reduces murine retinal cell death in vitro and in vivo. Journal of Pharmacology and Experimental Therapeutics, 332(2), 380–387. 10.1124/jpet.109.156612 [PubMed: 19910537]

Smith AW, Das A, Guyton MK, Ray SK, Rohrer B, & Banik NL (2011). Calpain inhibition attenuates apoptosis of retinal ganglion cells in acute optic neuritis. Investigative Ophthalmology and Visual Science, 52(7), 4935–4941. 10.1167/iovs.10-7027 [PubMed: 21613375]

Sorimachi H, Ishiura S, & Suzuki K (1997). Structure and physiological function of calpains. Biochemical Journal, 328(Pt 3), 721–732. [PubMed: 9396712]

Strobl S, Fernandez-Catalan C, Braun M, Huber R, Masumoto H, Nakagawa K, … Bode W (2000). The crystal structure of calcium-free human m-calpain suggests an electrostatic switch mechanism for activation by calcium. Proceedings of the National Academy of Sciences, 97(2), 588–592.

Suzuki K, Hata S, Kawabata Y, & Sorimachi H (2004). Structure, activation, and biology of calpain. Diabetes, 53(Suppl 1), S12–S18. [PubMed: 14749260]

Swerdlow NR, Braff DL, & Geyer MA (1999). Cross-species studies of sensorimotor gating of the startle reflex. Annals of the New York Academy of Sciences, 877, 202–216. [PubMed: 10415651]

Syntichaki P, Xu K, Driscoll M, & Tavernarakis N (2002). Specific aspartyl and calpain proteases are required for neurodegeneration in *C. elegans*. Nature, 419(6910), 939–944. 10.1038/nature01108 [PubMed: 12410314]

Thompson JD, Higgins DG, & Gibson TJ (1994). CLUSTAL W: Improving the sensitivity of progressive multiple sequence alignment through sequence weighting, position-specific gap penalties and weight matrix choice. Nucleic Acids Research, 22(22), 4673–4680. [PubMed: 7984417]

Trager N, Smith A, Wallace Iv G, Azuma M, Inoue J, Beeson C, & Banik NL (2014). Effects of a novel orally administered calpain inhibitor SNJ-1945 on immunomodulation and neurodegeneration in a murine model of multiple sclerosis. Journal of Neurochemistry, 130(2), 268–279. 10.1111/jnc.12659 [PubMed: 24447070]

Velez G, Bassuk AG, Colgan D, Tsang SH, & Mahajan VB (2017). Therapeutic drug repositioning using personalized proteomics of liquid biopsies. JCI Insight, 2(24), e97818 10.1172/jci.insight.97818.

Velez G, Tsang SH, Tsai YT, Hsu CW, Gore A, Abdelhakim AH, … Mahajan VB (2017). Gene therapy restores Mfrp and corrects axial eye length. Scientific Reports, 7(1), 16151 10.1038/s41598-017-16275-8 [PubMed: 29170418]

Velez G, Bassuk AG, Schaefer KA, Brooks B, Gakhar L, Mahajan M, … Mahajan VB (2018). A novel de novo CAPN5 mutation in a patient with inflammatory vitreoretinopathy, hearing loss, and developmental delay. Cold Spring Harbor Molecular Case Studies, 4, a002519 10.1101/mcs.a002519 [PubMed: 29472286]

Wang Y, Zhang X, Song Z, & Gu F (2017). An anti-CAPN5 intracellular antibody acts as an inhibitor of CAPN5-mediated neuronal degeneration. Oncotarget, 8(59), 100312–100325. 10.18632/oncotarget.22221 [PubMed: 29245980]

Wert KJ, Bassuk AG, Wu WH, Gakhar L, Coglan D, Mahajan M, … Mahajan VB (2015). CAPN5 mutation in hereditary uveitis: The R243L mutation increases calpain catalytic activity and triggers intraocular inflammation in a mouse model. Human Molecular Genetics, 24(16), 4584–4598. 10.1093/hmg/ddv189 [PubMed: 25994508]

Wert KJ, Davis RJ, Sancho-Pelluz J, Nishina PM, & Tsang SH (2013). Gene therapy provides long-term visual function in a preclinical model of retinitis pigmentosa. Human Molecular Genetics, 22(3), 558–567. 10.1093/hmg/dds466 [PubMed: 23108158]

Wert KJ, Mahajan VB, Zhang L, Yan Y, Li Y, Tosi J, … Tsang SH (2016). Neuroretinal hypoxic signaling in a new preclinical murine model for proliferative diabetic retinopathy. Signal Transduction and Targeted Therapy, 1, 1 10.1038/sigtrans.2016.5

Wert KJ, Sancho-Pelluz J, & Tsang SH (2014). Mid-stage intervention achieves similar efficacy as conventional early-stage treatment using gene therapy in a preclinical model of retinitis pigmentosa. Human Molecular Genetics, 23(2), 514–523. 10.1093/hmg/ddt452 [PubMed: 24101599]

Wert KJ, Skeie JM, Bassuk AG, Olivier AK, Tsang SH, & Mahajan VB (2014). Functional validation of a human CAPN5 exome variant by lentiviral transduction into mouse retina. Human Molecular Genetics, 23(10), 2665–2677. 10.1093/hmg/ddt661 [PubMed: 24381307]

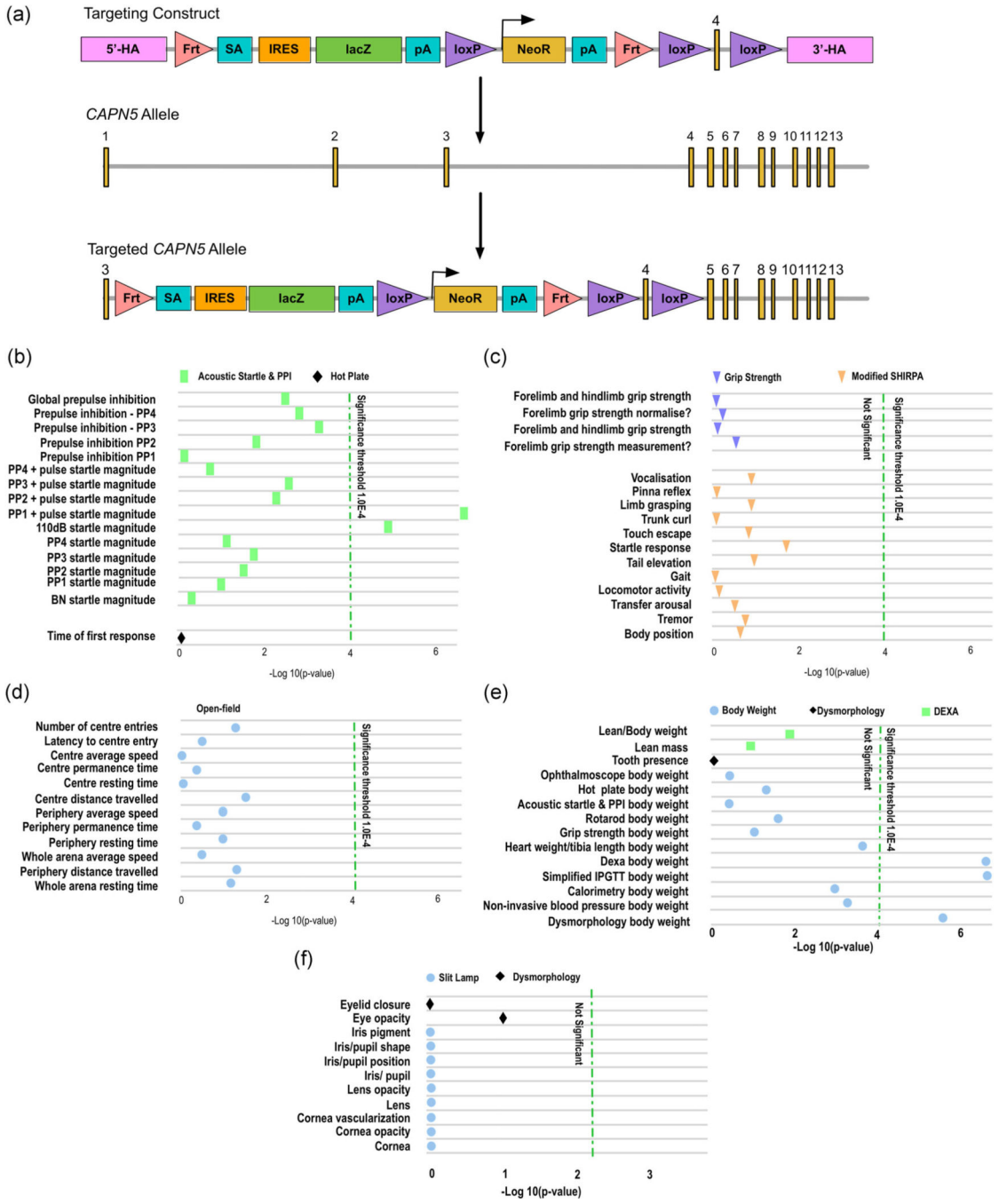

FIGURE 1.

Loss of *Capn5* may lead to hearing loss and increased body weight. We mined the current data on *Capn5* in the International Mouse Phenotyping Consortium (IMPC), Knockout Mouse Project (KOMP), EUCOMM (European Conditional Mouse Mutagenesis Program), and Mouse Genome Informatics (MGI) databases (Blake et al., 2017; Dickinson et al., 2016). (a) The *Capn5*$^{tm1a(EUCOMM)Hmgu}$ mice contain the tm1a targeting construct, consisting of a cassette containing the lacZ sequence flanked by an Frt and loxP site. This targeting construct was inserted into position 98136457 of chromosome 7, before exon 4 of

the *Capn5* allele. The targeted tm1a allele contains neomycin resistance (NeoR) followed by a loxP site driven by the human beta-actin promoter, followed by Simian Virus 40 (SV40), polyadenylation signal (pA), a second Frt site, and a second loxP site. Additionally, after the critical exon, exon 4 of *Capn5,* a third loxP site was inserted. 3′-HA, 3′ homology arm; 5′-HA, 5′ homology arm. (b) Both male and female homozygotes for the *tm1a* disrupted *Capn5* allele showed a significantly increased acoustic startle reflex and prepulse inhibition (PPI; $p < .0001$). Other neurological symptoms were not found to be significantly altered in the *Capn5* knockout mice, including (c) physical neurological defects and (d) mental neurological defects. (e) Both male and female homozygotes for the *tm1a* disrupted *Capn5* allele showed a significant increase in body weight ($p < .0001$). (f) No significant differences in the anterior eye of the mice homozygous for the *tm1a* allele in *Capn5* was detected

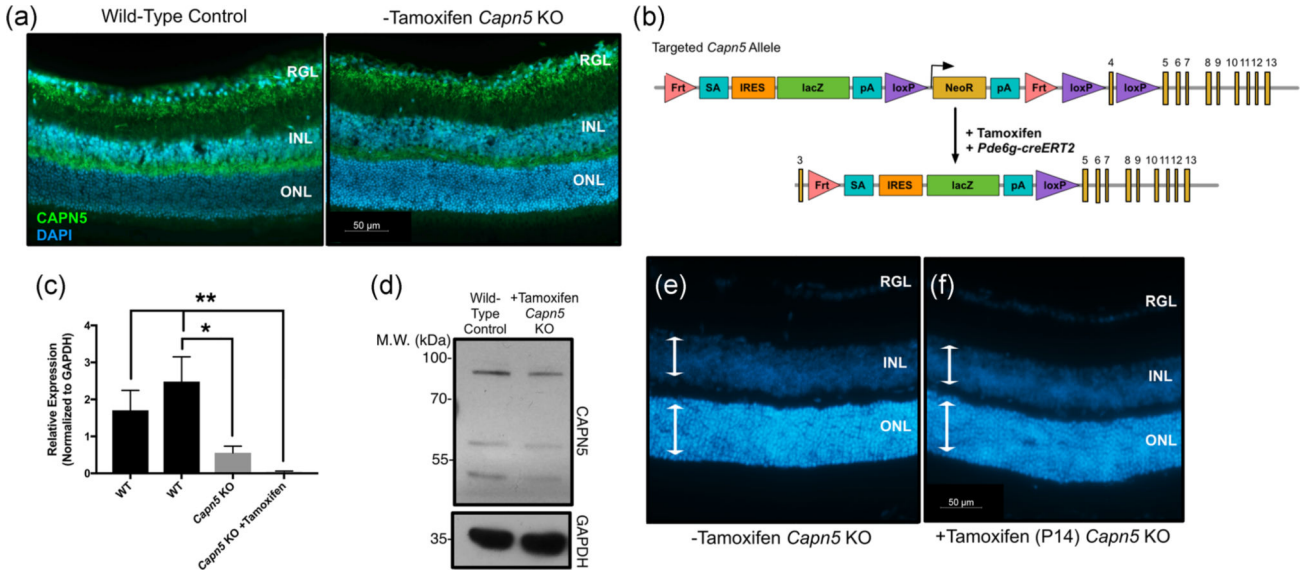

FIGURE 2.

Knockout of *Capn5* in the mouse photoreceptor cells leads to no detectable adverse clinical outcomes. (a) 2.5-month-old mouse eyes from wild-type (WT) and *Capn5* KO + tamoxifen mice were cross-sectioned from posterior–anterior axis including the optic nerve and stained for CAPN5 protein (green). DAPI (blue) highlights the nuclei. DAPI, 4′,6-diamidino-2-phenylindole; INL, inner nuclear layer; ONL, outer nuclear layer; RGL, retinal ganglion cells. (b) The targeting construct for our *Pde6g-creERT2* mouse line (Koch et al., 2015, 2017). One allele of phosphodiesterase 6γ *(Pde6g)* contains a cassette with *creERT2* before exon 4, which is activated by delivery of tamoxifen. 3′-HA, 3′ homology arm; 5′-HA, 5′ homology arm; EM7, bacteriophage T7 promoter; bGHpA, bovine growth hormone polyadenylation signal; NeoR, neomycin resistance; pA, polyadenylation signal; PGK, phosphoglycerate kinase promoter; TK, thymidine kinase. (c) The targeted tm1a allele in *Capn5* KO mice after being crossed with the *Pde6g-creERT2* mice and after delivery of tamoxifen ensures a loss of the critical *Capn5* exon 4. (d) Retinas were dissected at postnatal Day 42 (P42) and genomic DNA was extracted. Quantitative polymerase chain reaction (qPCR) was performed for *Capn5* expression in the *Capn5* KO mice and *Capn5* KO +tamoxifen mice compared to two WT control samples (Far left, 129/SvEV agouti; second to the left, C57BL/6J). Samples were run in triplicate, normalized to *Gapdh,* and error bars represent the standard deviation between triplicates. The *Capn5* KO retina was significantly decreased compared to the C57BL/6J WT sample ($p = .0049$). The *Capn5* KO +tamoxifen retina was significantly decreased compared to both WT samples ($p = .0104$ and $p = .0014$, respectively). (e) Western blot analysis of CAPN5 using 2-month-old retinal lysates from WT (left lane) and Capn5 KO +tamoxifen (right lane) mice. GAPDH was used as a loading control. P42 mouse eyes from (f). *Capn5* KO mice and G. *Capn5* KO + tamoxifen mice were cross-sectioned from posterior–anterior axis including the optic nerve, stained with DAPI to highlight the nuclei, and retinal sections were magnified to examine thickness of retinal cell layers. White arrows, thickness of the INL/ONL, same size across both images. $N \geq 4$ mice for all mouse experimental groups. GAPDH, glyceraldehyde 3-phosphate dehydrogenase; INL, inner nuclear layer; KO, knockout; ONL, outer nuclear layer

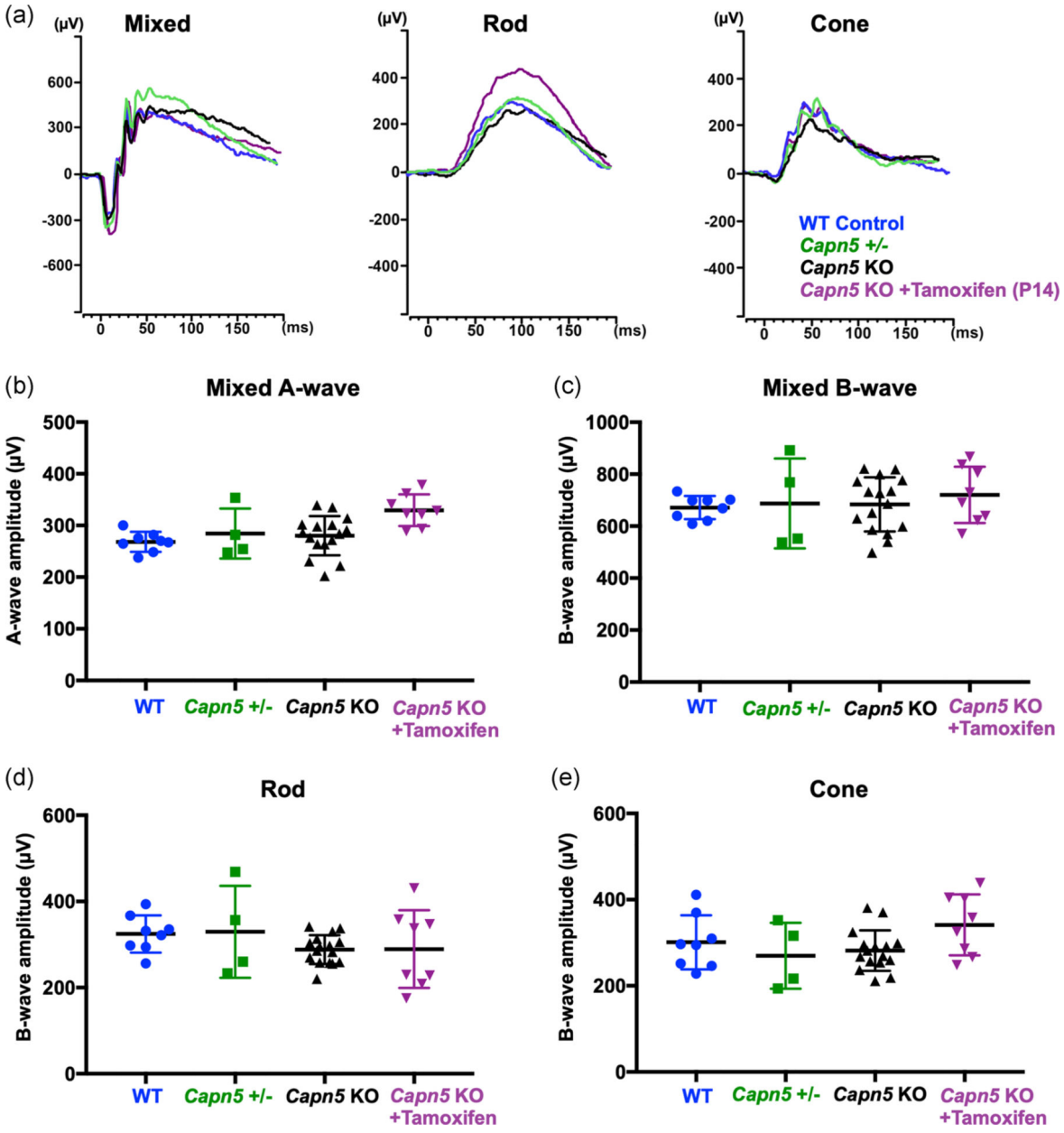

FIGURE 3.

No major electrophysiological changes in vision after the loss of *Capn5* in the photoreceptor cells. At approximately one month of age, retinal function was analyzed by electroretinogram (ERG) for C57BL6/J wild-type mice (WT; blue), *Capn5* heterozygous mice (*Capn5*$^{+/-}$; green), *Capn5* knockout (KO) mice (black), and in *Capn5* KO + tamoxifen mice (purple). (a) Representative traces were shown for the scotopic mixed rod–cone signal (left), the scotopic rod-specific signal (middle), and the photopic cone-specific signal (right). Quantification of ERG amplitudes for (b) the mixed rod–cone-specific a-wave, (c) the mixed rod–cone-specific b-wave, (d) the scotopic rod-specific b-wave, and (e) the photopic cone-specific b-wave. One-way analysis of variance followed by Tukey's post-hoc multiple comparison's test was performed to compare each group. $p = .0056$ for the mixed rod–cone-

specific a-wave (WT vs. *Capn5* KO + tamoxifen, $p = .0062$; *Capn5* KO vs. *Capn5* KO + tamoxifen, $p = .0115$); $p = .8056$ for the mixed rod–cone-specific b-wave; $p = .4045$ for the scotopic rod-specific b-wave; $p = .1179$ for the photopic cone-specific b-wave. Dots, squares or triangles represent individual eyes, black lines represent the group means. Bars display the standard error of the mean. $N = 8$ (WT), 4 *(Capn5*$^{+/-}$*),* 16 *(Capn5* KO), and 8 *(Capn5* KO + tamoxifen) samples

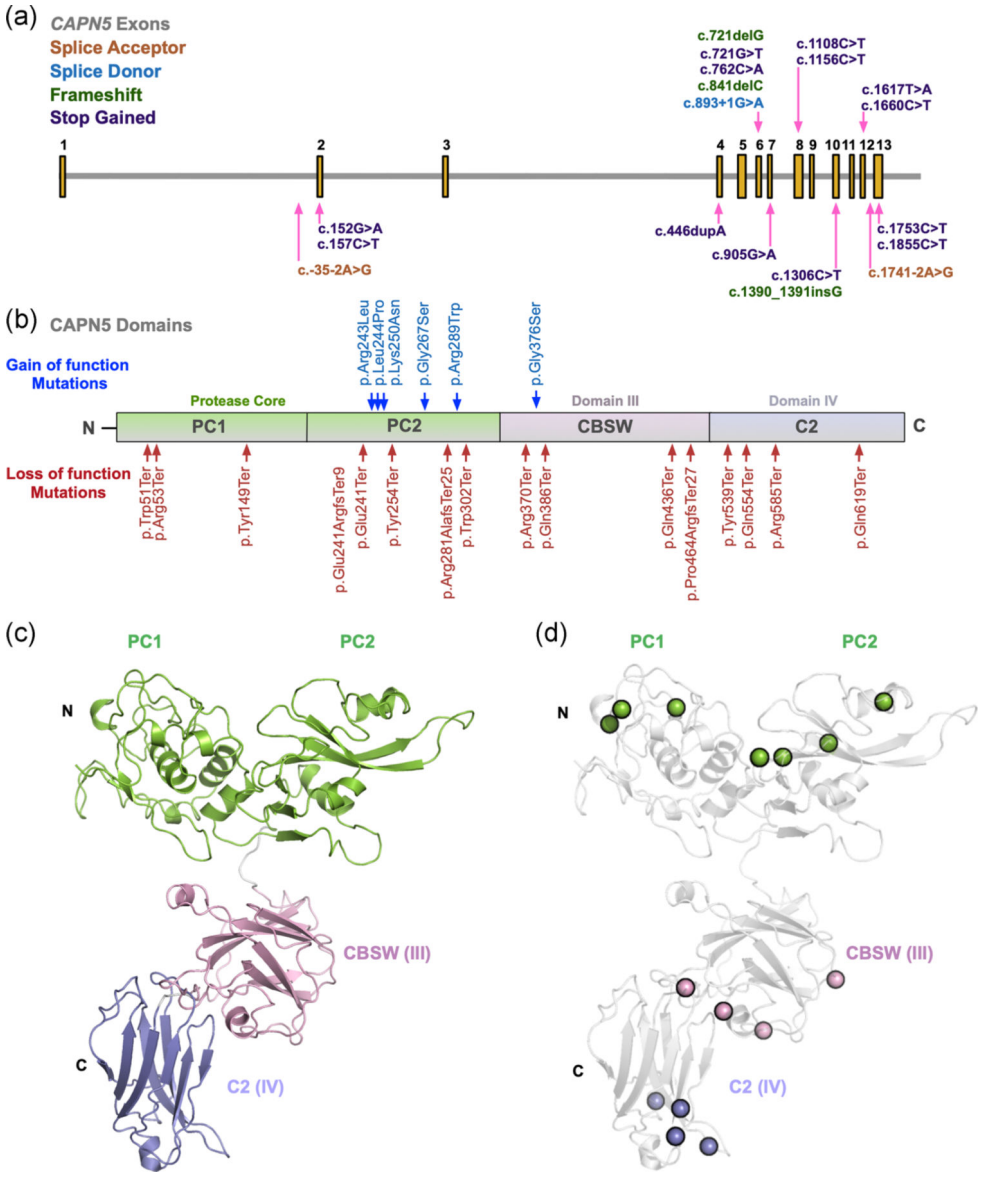

FIGURE 4.

Structural modeling of calpain-5 splice-site variants and coding mutations. (a) Using the Exome Aggregation Consortium (ExAC) data set (ENSG00000149260), the location of each splice-site (acceptor, orange; donor, blue) and coding (frameshift, green; stop gained, purple) loss-of-function (LOF) variant from the canonical transcript for calpain-5 *(CAPN5)* is mapped on chromosome 11. (b) CAPN5 LOF variants (red) and published autosomal dominant neovascular vitreoretinopathy (ADNIV) gain-of-function (GOF) variants (blue) were mapped along the protein structure of CAPN5. CAPN5 protein structure contains an N-terminal tail, the protease core (PC1 and PC2, green), a regulatory calpain β-sandwich domain (CBSW; DIII, pink) and a C2 domain (DIV, blue). (c) A model of the full-length CAPN5 protein was generated using a domain assembly approach. Models of the individual domains were then assembled using ab initio domain assembly in MODELLER to generate

a model of the full-length CAPN5 structure. (d) The location of LOF coding variants on CAPN5's domains were mapped to the structural model

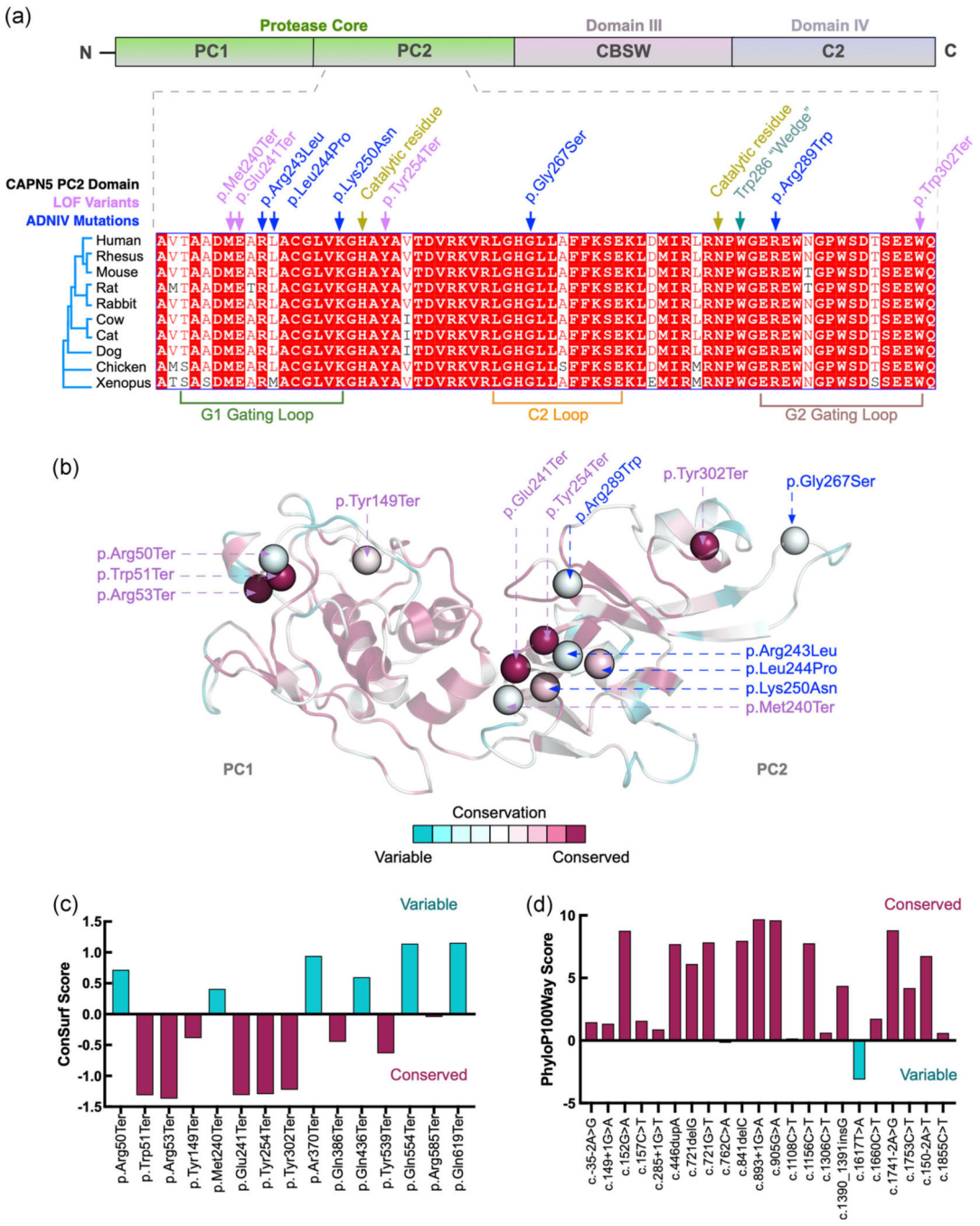

FIGURE 5.

High conservation of variant sites in *CAPN5* between invertebrates and vertebrates. (a) Human amino acid sequences from the protease core of CAPN5 (PC2, purple, dashed lines) were aligned to nine specific vertebrates: rhesus, mouse, rat, rabbit, cow, cat, dog, chicken, and xenopus. CAPN5 loss-of-function (LOF) variants (purple) were found in highly conserved regions alongside published autosomal dominant neovascular inflammatory vitreoretinopathy (ADNIV)-disease-causing gain-of-function (GOF) variants (blue). (b) ConSurf conservation analysis using our structural model of CAPN5 as input and

comparison to 150 closest homologs including both invertebrates and vertebrates. ConSurf conservation scores were mapped onto our protease core (domain PC2) structural model of CAPN5. (c) Conservation scores were plotted for each of the LOF variants within the protease core (PC2) from 150 analyzed homologs (negative indicates conserved, positive indicates variable amino acid positions). (d) Each of the 22 LOF gene variants for human *CAPN5* was used as input into the 100 vertebrate base-wise conservation by PhyloP (phyloP100way). Variants with high conservation, magenta; variants with low conservation, cyan

TABLE 1

Human loss-of-function variants in *CAPN5*

Function	Transcript change	Protein change	Allele frequency	Allele count	Allele number	Number of homozygotes	Noncanonical transcript
Stop gained	c.762C > A	p.Tyr254Ter	0.0001453	17	117032	0	–
Stop gained	c.1617T > A	p.Tyr539Ter	0.00006292	6	95366	0	–
Stop gained	c.157C > T	p.Arg53Ter	0.0000518	6	115820	0	–
Stop gained	c.152G > A	p.Trp51Ter	0.00003439	4	116314	0	–
Stop gained	c.1306C > T	p.Gln436Ter	0.0000338	4	118350	0	–
Stop gained	c.1108C > T	p.Arg370Ter	0.00003068	3	97770	0	–
Stop gained	c.1753C > T	p.Arg585Ter	0.00002496	3	120174	0	–
Stop gained	c.1156C > T	p.Gln386Ter	0.00002268	1	44092	0	–
Stop gained	c.1660C > T	p.Gln554Ter	0.00001655	2	120850	0	–
Stop gained	c.905G > A	p.Trp302Ter	0.00001053	1	94930	0	–
Stop gained	c.721G > T	p.Glu241Ter	0.000009028	1	110770	0	–
Stop gained	c.446dupA	p.Tyr149Ter	0.000008259	1	121074	0	–
Stop gained	c.1855C > T	p.Gln619Ter	0.00000825	1	121206	0	–
Frameshift	c.841delC	p.Arg281AlafsTer25	0.00003388	4	118052	0	–
Frameshift	c.721delG	p.Glu241ArgfsTer9	0.00001816	2	110154	0	–
Frameshift	c.1390_1391insG	p.Pro464ArgfsTer27	0.000008246	1	121268	0	–
Splice acceptor	c.150−2A > T	–	0.0003796	46	121176	0	Yes
Splice acceptor	c.–35 − 2A > G	–	0.00002581	3	116246	0	–
Splice acceptor	c.1741 − 2A > G	–	0.000008385	1	119258	0	–
Splice donor	c.285 + 1G > T	–	0.002916	25	8574	1	Yes
Splice donor	c.149 + 1G > A	–	0.00005151	6	116476	0	Yes
Splice donor	c.893 + 1G > A	–	0.00001808	2	110624	0	–

Note: We interrogated the Exome Aggregation Consortium (ExAC) browser for human *CAPN5* (ENSG00000149260; GRCh37/hg19; chr11:76777979–76837201). We found 880 variants, 22 of which were considered loss-of-function (LOF) variants for *CAPN5* and tolerable in the human population.